Journal of Applied Polymer Science

Microstructure and Properties of Branched Polyethylene: Application of a Three-Phase Structural Model

S. Martín, M. T. Expósito, J. F. Vega, J. Martínez-Salazar
Departamento de Física Macromolecular, Instituto de Estructura de la Materia, CSIC Serrano 113 bis, 28006 Madrid, Spain
Correspondence to: J. F. Vega (E-mail: jfvega@iem.cfmac.csic.es)

ABSTRACT: A combined study of microstructure and mechanical properties for a series of single-site metallocene ethylene/1-hexene copolymers is presented. The analysis of the results focuses on the effect of branching, which in turn modulates crystallinity and density, on the values of the elastic modulus obtained in tensile-deformation experiments. An extensive literature review is done in order to compare our own results with previous studies. The typical variation found in the elastic modulus is discussed in terms of the existence of a rigid amorphous phase. This rigid phase controls the macroscopic mechanical behavior of the materials, giving rise to an increase of the elastic modulus as the crystallinity does. Mechanical coupling models for heterogeneous systems are applied in order to describe the experimental results of the elastic modulus as a function of the variation of three different phase fractions, i.e., crystalline, rigid amorphous (or interfacial), and mobile amorphous. The phase fraction values obtained from the analysis of the mechanical properties are in qualitative agreement to those found experimentally in our group by Raman infrared spectroscopy and from the literature by positron annihilation lifetime spectroscopy. © 2012 Wiley Periodicals, Inc. J. Appl. Polym. Sci. 000: 000–000, 2012

KEYWORDS: polyolefins; microstructure; mechanical properties; copolymers

Received 5 August 2010; accepted 3 July 2012; published online
DOI: 10.1002/app.38290

INTRODUCTION

The basis of the specific macroscopic properties of semicrystalline polymers lies on their hierarchical structure.[1] Molecular features and chemical composition strongly affect macromolecular organization at the nano- and microscopic levels. The large compositional variety achievable by copolymerization generates polymeric materials with very different microstructures, and then with a wide range of physical properties. In these materials, the extensively studied uniaxial tensile patterns change from the typical plastic behavior of highly crystalline thermoplastics to the elastomeric behavior of low crystallinity polymers.[2–11] However, the heterogeneous molecular population, mainly dependent on the polymerization process, and the complex microstructural features of these semicrystalline systems have veiled the understanding of the microscopic mechanisms underlying the deformation processes. Of the same importance than the molecular features are the crystallization conditions that define the degree of macromolecular order in the materials. Then, molecular features and crystallization conditions should be controlled to obtain reliable correlations between structural features and macroscopic properties.

The development of the single-site catalyst technology has allowed for the synthesis of olefin-based linear homo and copolymers with narrow molecular weight distribution and homogeneous branching distribution. In addition, this technology yields polymers with a large incorporation of comonomer, offering a broad range of solid-state structures and physical properties. Our group has previously explored these macromolecular models in order to establish basic correlations between molecular architecture, microstructure, and physical properties using both advanced computer simulations[12,13] and experimental approaches.[14–18] Some works can be found in the literature concerning the physical properties of polyethylene fractions and model monodisperse hydrogenated polybutadiene,[5,7,8] but limited to a narrow range of materials' density and/or molecular weight. More recent works describe the structure–properties relationship in homogeneous series of ethylene/1-octene and ethylene/styrene copolymers obtained by means of single-site constrained geometry catalyst systems.[19]

In the context of the relationship between microstructural features and physical properties, some authors have suggested the existence of an amorphous rigid phase, associated with both the mobile amorphous and the crystalline phases, and with intermediate properties,[20–22] whereas others identified this third phase as an interfacial layer between the crystalline and the amorphous material.[23] Raman infrared spectroscopy has been

Table I. Branching Content, Weight Average Molecular Weight, Polydispersity Index, Density, Glass Transition Temperature, Melting Point, Mass Fractional Crystallinity, and Elastic Modulus of the Samples Investigated

Sample	Branching CH_3/1000 C	M_w (kg mol^{-1})	M_w/M_n	ρ (g cm^{-3})	T_g (°C)	T_m (°C)	w_{DSC}	E (MPa)
EH0	0	158	2.0	0.9516	-	134.2	0.70	874 ± 32
EH3	2.80	124	2.0	0.9382	-	125.9	0.62	590 ± 25
EH5	5.35	115	2.0	0.9311	-	121.4	0.57	451 ± 20
EH8	8.10	126	2.0	0.9256	-	120.7	0.55	378 ± 20
EH10	9.60	113	2.0	0.9222	-	116.3	0.52	300 ± 18
EH15	15.0	200	2.1	0.908	−36.1	106.7	0.40	166 ± 6.0
EH23	23.3	350	2.0	0.891	−45.4	97.9	0.33	60.6 ± 2.4
EH35	35.7	370	2.0	0.879	−53.8	75.3	0.27	29.7 ± 1.1
EH42	42.0	340	2.1	0.871	−58.4	66.4	0.22	17.7 ± 0.6
BL3	1.40	-	-	0.9441	-	130.6	0.66	745 ± 30
BL5	2.68	-	-	0.9397	-	128.5	0.64	668 ± 27
BL8	4.05	-	-	0.9374	-	128.8	0.61	597 ± 21
BL10	4.80	-	-	0.9358	-	127.5	0.60	559 ± 21

widely used since the 80s in order to study these microstructural aspects of polyolefins, and more precisely to identify the interfacial region between the amorphous and crystalline phases.[24–26] The results obtained by positron annihilation lifetime spectroscopy (PALS) also suggest the existence of a rigid amorphous phase in this type of materials.[27–29] It is clear that the phase structure and the coupling between the phases modulate the mechanical properties of this important class of materials. The chain segmental mobility of the amorphous regions is gradually decreased as crystal volume in the systems increases. As reported in the literature, chain mobility restrictions in semicrystalline systems can be observed by means of dynamic mechanical thermal analysis (DMTA) or broadband dielectric spectroscopy (BDS) through the changes in the segmental relaxation processes.[30–32] In this respect, the recent development of a statistical model, which accounts for the thermodynamic changes in the amorphous regions due to the presence of the crystals, describes the effect of the confinement on chain conformation dynamics.[33,34]

In this work, we have investigated the mechanical behavior of high molecular weight single-site metallocene ethylene/1-hexene homogeneous copolymers with narrow molecular weight distribution. One set of the materials, in the usual commercial range of comonomer content from 0 to 2 mol %, have been obtained from Repsol-YPF (Móstoles, Spain). The other set of materials have been synthesized in our laboratory, covering an unusual low crystallinity range controlled by varying the comonomer incorporation during the polymerization process. The materials cover the comonomer content range between 3 and 10 mol %. One important objective of this work is to examine the effect of branching in the mechanical tensile-deformation behavior. The other is the application of coupling models to experimental data, in order to explain the mechanical response of the materials from a structural point of view.

EXPERIMENTAL

Materials and Sample Preparation

The copolymers are designated as EHx, being x the amount of short chain branching determined by ^{13}C-NMR. The branching level and the molecular features obtained by size exclusion chromatography are listed in Table I for all the materials studied. Please refer to previous works for details about materials synthesis and molecular characterization.[3–6] A set of blends between the linear sample (EH0) and the branched samples with the lowest branching content (EH3–EH10) have been also studied. The blends (50/50 wt %) were prepared in a Custom Scientific Instruments Mini-Max CSL mixer (Easton PA) at a temperature of 160°C and a piston speed of 60 r.p.m for 15 min. Densities, measured in a gradient column at 23°C, are also reported in Table I. The polymers (stabilized against thermo-oxidative degradation) were melt pressed in a Schwabenthan Polystat 200 T laboratory hot press (Berlin, Germany) at 150°C temperature and 50 bars of nominal pressure for 5 min, adjusting the thickness to a suitable one to the intended experiments. The sheets were quenched at room temperature.

Differential Scanning Calorimetry

The thermal characterization was performed in samples with the same heat and strain history than those used in the subsequent tensile-deformation testing. Thermal characterization of the samples was conducted in a Perkin Elmer Pyris 1 calorimeter (Waltham, MA) in helium atmosphere and cooling liquid nitrogen supply. Temperature calibrations were made using the melting onset of water and indium. The masses were weighed in a Perkin Elmer high precision scale with an accuracy of 0.001 mg. The polymers were cooled to −150°C at 100°C/min and immediately heated up to 150°C at two heating rates: 10°C/min and 40°C/min. Subsequent cooling and heating cycles on the quenched samples were also performed in the same conditions. The contribution of an empty pan was subtracted from each

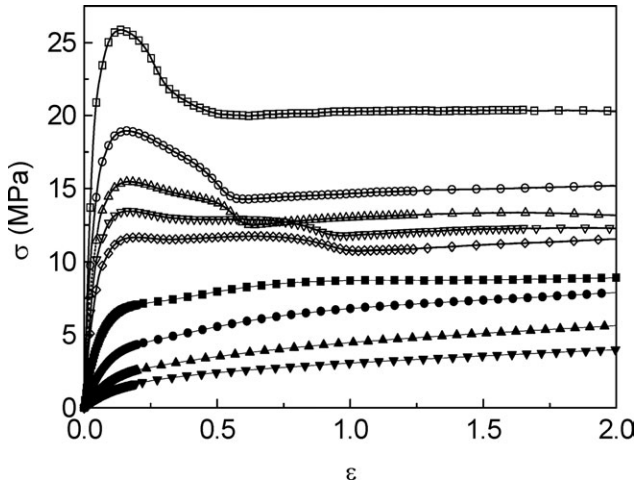

Figure 1. True stress–strain curves for the materials studied: (□) EH0, (◯;) EH3, (△) EH5, (◊) EH10, (■) EH15 (●) EH23, (▲) EH35 (♦) EH42.

experiment. The glass transition temperature (T_g) was determined from the heat flow curves. The melting temperature (T_m) was defined as the maximum peak of the melting endotherm. Please refer to Ref. 18 for details. The degree of the mass fraction of crystals was calculated as $w_{DSC} = \Delta H_m/\Delta H_m^0$, where ΔH_m is the melting enthalpy of the samples and ΔH_m^0 is the equilibrium melting enthalpy of a completely crystalline polyethylene taken to be 288.4 J/g.[35] The specific heat capacity is not constant in polyolefins, being a function of the temperature,[36] then we have corrected the values of ΔH_m using the heat of fusion values determined by Wild et al. in preparative fractions of 1-butene copolymer as a function of their melting temperature.[37] All the thermal properties, corrected for a heating rate of 0 °C/min, are listed in Table I.

Tensile deformation experiments

Specimens were stamped out from hot press molded μm thickness sheets. The "dog-bone" specimens' dimensions were 35 mm length and 6 mm width, with a gauge length of 12 mm. An Instron machine model 1122 (Norwood, MA) equipped with a 500 N tension load cell was employed for tensile testing. The cell was calibrated with different standards. All tensile tests were conducted at a temperature of 23°C and 50% humidity, with a crosshead speed of 10 mm/min. The nominal force was measured by the load cell, and the nominal stress, σ, calculated dividing by the initial sectional area of the specimens. The deformation was carried out to fracture of the samples. The nominal strain, ε, was measured as the crosshead displacement divided by the original gauge length of 12 mm.

Raman Infrared Spectroscopy

Raman spectra of the ethylene/1-hexene samples were recorded at 23°C using a Renishaw microscope system RM2000 (Gloucestershire, UK) equipped with an optical Leica microscope (Heerbrugg, Switzerland) and an Argon ion laser at 514 nm as the light source. Each spectrum was based on 20 scans with ×50 magnification objective lenses.

RESULT AND DISCUSSION

For the copolymers studied, the peak melting temperature (T_m) and mass crystal content (w_{DSC}) decrease with increasing comonomer content (see Table I). These trends reflect the exclusion of the comonomer from the crystal and the progressive decrease in the length and concentration of crystallizable ethylene sequences. We also observe that as the branching content increases, the values of the glass transition temperature (T_g) decrease. This fact has been associated with an increase of the free volume of the amorphous phase developing in the polymers as crystallinity decreases.

It is not expected any important change in the shape of the stress–strain tensile curves due to the differences in the molecular weight,[9] but the different branching content should lead to important variations in mechanical properties. In Figure 1 we can realize that the reference linear homopolymer sample (EH0) is characterized by a sharp and well-defined yield. By increasing the branching content, there is a continuously decreased yield stress maximum. In fact, in the sample with 15 branches/1000 C atoms no yield is present. Above this value of the branching content, the polymers show a characteristic rubber-like behavior: the stress level is substantially reduced relative to the reference homopolymer or the copolymers with a lower branching degree. The elastic modulus, E (see Table I), has been determined from the slope of the force–elongation curve in the limit of very small strain where the deformation is reversible (lower than 0.2). In this region, it is supposed that the disordered entangled structure is involved in the deformation process, but the ordered crystalline structure is no longer affected.

We have first concentrated our attention on the influence of crystal content in the values of E, considering a simple 2-phase model. Figure 2 is a plot of E against the volume crystalline fraction, α. Densities of 1 g/cm^3 and 0.856 g/cm^3 for the crystalline and amorphous phases have been considered for calculations of α from the corrected results of the mass crystallinity

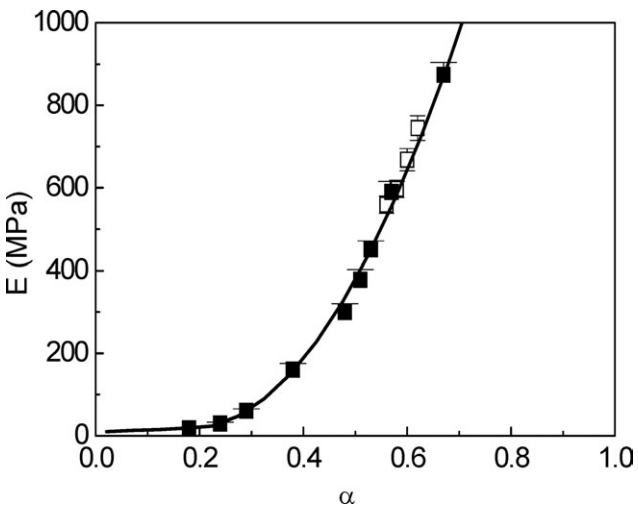

Figure 2. Elastic modulus as a function of crystalline fraction for the different samples studied (■) and blends of the linear and branched samples (□).[38]

Applied Polymer SCIENCE

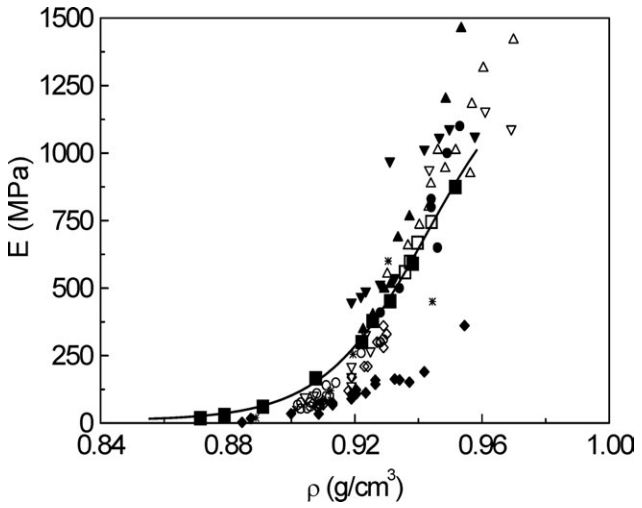

Figure 3. Elastic modulus as a function of sample density for the pure materials studied (■), the blends of linear and branched samples (□)[38] (the line has been drawn to guide the eye); and for different samples from the literature. Ref. 2: branched PE samples (▲). Ref. 3: Ziegler–Natta PE samples (*). Ref. 4: Linear PE samples (▼) and branched PE samples (▽). Ref. 5: NBS Linear PE samples (●); hydrogenated poly-butadiene (HPB) linear and star samples (◯); and HPB linear-linear and linear-star blends (◊). Ref. 6: single-site catalysts ethylene/α-olefin copolymers (♦). Ref. 17: single-site catalyst linear PE samples (△).

content obtained by DSC. The density of the amorphous phase has been considered independent of the amount of comonomer. A linear dependence between E and α is obtained for high crystallinity, but a clear breakdown is observed for volume crystallinity fractions lower than $\alpha = 0.4$. In fact, an asymptotic dependence of the elastic modulus to the typical values of rubber-like materials at room temperatures around 10 MPa for $\alpha = 0$ is found.[5,9,39] An extensive literature review has been done in order to compare these results with those corresponding to other polyolefins obtained from different sources.[2–6,11] The comparison is observed in Figure 3, where the elastic modulus is plotted against materials' density, ρ. Obviously, the scattering found among the collected data is likely due to differences not only in the molecular architecture (most of the polymers are polydisperse and, likely with a heterogeneous branching distribution), but also to differences in the sample preparation conditions. In this plot, density becomes as a structural parameter that monitors the mechanical behavior, independently of the nature of the comonomer (1-butene, 1-hexene or 1-octene) and the molecular topology, i.e., the presence of long chain branching, which is typical of some of the samples from the literature. We have to point out that the correlation obtained in our samples nicely follows a single correlation among all the collected data.

Results obtained in the blends of linear and moderate branched samples are included in Figures 2 and 3. These blends show volume crystalline fractions higher than $\alpha = 0.4$, and a melting behavior driven by the linear species, as judged by the results shown in Table I.[38] The blends show higher T_m values for similar crystalline content than the pure EH copolymers with the same average short chain branching content, suggesting larger lamellae dimensions. However, the elastic modulus seems to follow the same linear trend than the pure EH copolymers. This result demonstrates that other feature than the crystal thickness is playing a role in the values of the elastic modulus.[8,9] Moreover, the reversibility of the deformation at the very small strain region at which the elastic modulus is determined is an indication that the amorphous entangled fraction is playing an important contribution to the modulus. The strong variation in the elastic modulus of the materials can be ascribed then to strong changes in the amorphous fraction: the stiffness of the amorphous component should drop appreciably as the branching content decreases. The glass transition temperature in these semicrystalline samples has shown a strong dependence of the branching content (see Table I), suggesting a higher free volume due to the presence of branches. Rheological measurements also point toward substantial changes of the entangled structure in the amorphous melt state due to an increased branching content, but the changes are only 2-fold lower than for the linear homopolymer, which is not enough to explain the huge change observed in Figure 2.[15,40,41] A simple combination of the corresponding extrapolated crystalline (100% crystallinity) and amorphous (0% crystallinity) moduli and phase volume fractions is not able to explain the sudden change in the properties observed within the crystallinity range below $\alpha = 0.4$. Then, the mechanical properties should be a consequence of the combination of factors related not only to the amount of crystals but also to the nature of the amorphous phase.

Following these ideas, it can be argued that the changes in the amorphous regions due to the different crystal content in the samples control the mechanical behavior. It is usual to describe the variation of properties of semicrystalline polymers with simple 2-phase mechanical models. Several semi-empirical approaches have been proposed in order to represent the experimental moduli. Among them, the "mean field approximations" developed by Kerner, Hashin-Rosen and Tsai-Halpin have been shown to explain the behavior of polyethylene with crystallinity independent parameters in the crystal content range $\alpha > 0.4$.[42] The Tsai-Halpin equation for the tensile modulus has been also probed to describe the mechanical behavior of semicrystalline polyethylene in this crystal content range:[39]

$$E = \frac{E_a[E_c + \xi(\alpha E_c + (1-\alpha)E_a)]}{\alpha E_a + (1-\alpha)E_c + \xi E_a} \quad (1)$$

where E_c and E_a are the moduli of the crystalline and amorphous phases having volume fractions α and $(1 - \alpha)$, respectively, and ξ is the reinforcement factor or contiguity factor of the filler (crystalline phase). Polymeric materials processed by traditional methods should show ξ values of the order of unity or less.[39,43,44] The Reuss inverse rule of mixtures for heterogeneous materials is recovered for $\xi = 0$. On the other hand, the Voigt averaging is obtained for very high values of ξ. The value of E_c is well established in the literature at around $E_c \sim 7$ GPa at room temperature,[45–47] while values of around $E_a \sim 10$ MPa can be found for fully amorphous polyethylene.[3,9] With these values in hand for the elastic modulus of the pure phases, the mechanical properties of the samples studied here cannot be described by means of eq. (1), nor using the Voigt neither

the Reuss averages. This result has been taken in the literature as an evidence of changes in E_a with crystallinity.[5] The high crystalline portion of the curve ($\alpha >> 0.5$) can be adequately described with a constant value of the amorphous modulus of E_a ~310 MPa in this region, by considering the Reuss averaging rule with $\xi = 0$, in agreement with the result obtained by Crist et al. for the modulus of the rigid amorphous region (E_{ar} 300 MPa).[5] Experimental observations suggest that the amorphous fraction of semicrystalline polymers is characterized by a heterogeneous structure due to the presence of crystallites, which reduce locally the molecular mobility of the disordered regions. A first approximation to illustrate this heterogeneity from the microscopic point of view consists on a classification of the disordered phase in "confined amorphous segments" with a reduced mobility, and "mobile amorphous segments" corresponding to the chain segments in the rubber-like state. This assumption led to some authors to suggest the existence of two glass transitions, one corresponding to the mobile free segments, and a higher one, corresponding to the hindered segments close to the crystals.[20] This has been recently probed for some polymers like poly(4-methyl-1-pentene) and poly(norbornene).[23] However, in the case of polyolefins applies better the notion of an "extended glass transition," developed by Struik: in a semicrystalline polymer the amorphous phase will have a broad T_g-distribution, as a consequence of a distribution of rigidities of the amorphous phase.[48,49] The lowest temperature of the distribution will correspond to the more flexible material fraction, and the highest will depend not only on the nature of the amorphous phase, but also on its interaction with the crystals. The existence of this confined or rigid amorphous phase, but associated with both a more mobile amorphous fraction and the crystalline structure and with intermediate properties, has been suggested by a number of authors,[20–23,48,49] whereas others identified this third phase as an interfacial layer between the crystalline and the amorphous material.[24]

A model based on the Reuss inverse mixing rule was suggested by Takayanagi et al. to account for the reinforcement effect in the mechanical properties of semicrystalline polymers:[50,51]

$$\frac{1}{E} = \frac{1-\alpha}{\psi E_c + (1-\psi)E_a} + \frac{\alpha}{E_c} \quad (2)$$

The model takes into account the one-dimensional lamellar structure with alternation of crystalline and amorphous layers. Then, the crystalline part occupies a volume fraction α, and the amorphous part occupies a volume $1 - \alpha$, with the contribution of two-component parallel layers of $1 - \psi$ volume fraction of amorphous material and ψ volume fraction of tie-taut molecules. In this model, ψ acts as the additional reinforcement parameter of the amorphous phase, and then it takes into account the variation of the amorphous modulus, depending on the amount present of a rigid or interfacial layer between both the amorphous mobile and crystalline phases. In Figure 4 we have plotted E as a function of crystallinity according to eq. (2), and substituting the corresponding values of $E_c = 7$ GPa and $E_a = 10$ MPa. The consideration of ψ as a constant did not give to agreement between the model and the experimental results, as it can be observed in the figure for $\psi = 0.045$ (fits only the high-branch of α) and $\psi = 0.0015$ (fits only the low-branch of α).

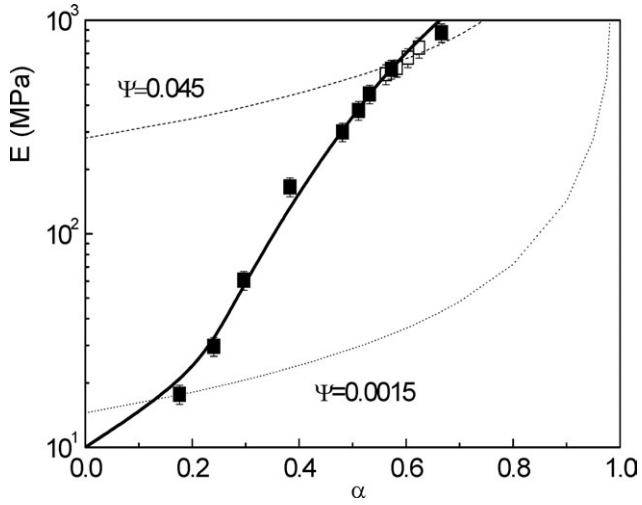

Figure 4. Application of the Takayanagi model [eq. (2)] to the experimental data of the elastic modulus (■) for two values of ψ to the elastic modulus of the samples studied (dashed and dotted lines), and considering variable ψ with the crystalline content (solid line). The solid line represents the best fit to the experimental elastic modulus with $E_c = 7$ GPa, $E_{ar} = 310$ MPa, and $E_{am} = 10$ MPa.

Then, the model is only able to describe the experimental data if a variation of ψ with the crystallinity is considered. Additionally, the rigid phase should contribute to the amorphous modulus with a value of around $E_{ar} = 310$ MPa [formerly $E_c = 7$ GPa in first term of the left-side hand of eq. (2)], as it was pointed out by Crist et al.[5] The physical meaning of E_c in the second term of the right-hand side of eq. (2) and α remains the same.

$$\frac{1}{E} = \frac{1-\alpha}{\psi E_{ar} + (1-\psi)E_a} + \frac{\alpha}{E_c} \quad (3)$$

We have now a mechanical model describing the coupling of the three different phases in the polymeric system: the amorphous phases are coupled in series, and both in parallel with the crystalline filler. The result of the application of the model can be observed also in Figure 4. As a result of the fitting (values of ψ as a function of α), we can obtain the rigid amorphous $\alpha_r = \psi(1 - \alpha)$ and the mobile amorphous $\alpha_m = (1 - \psi)(1 - \alpha)$ fraction for each material.

It is possible now to compare the values obtained from the model for each of the phases with those obtained experimentally. Raman infrared spectroscopy has been widely used since the 80 s in order to study the microstructure of semicrystalline polymers, but more precisely to identify and characterize the interfacial layer in semycrystalline polyolefins.[24–26] Other studies have obtained signatures of the rigid amorphous phase in ethylene/α-olefin copolymers by PALS.[27–29] The question that arises is whether the results obtained from the fitting to the mechanical properties could be related to the so-called interfacial or rigid amorphous phase measured in Raman infrared spectroscopy and PALS in ethylene/α-olefin copolymers. Following the procedure developed by Mutter and coworkers, the fraction of the different phases in the samples studied can be obtained from the observed intensities in the internal mode region of the

Table II. Mass Fraction of the Different Crystalline, Rigid (Interfacial), and Mobile Components in the Samples Studied Obtained by Raman Spectroscopy

Sample	X_c	X_r	X_m
EH0	0.66	0.21	0.12
EH3	0.58	0.25	0.17
EH5	0.48	0.34	0.18
EH8	0.41	0.37	0.22
EH10	0.38	0.38	0.24
EH15	0.29	0.34	0.36
EH23	0.20	0.26	0.54
EH35	0.08	0.19	0.72
EH42	0.04	0.12	0.84

Raman spectrum (600–1600 cm^{-1}).[52–54] Information about the results obtained in Raman experiments for the same samples studied here can be found in a previous work made in our group.[16] Overlapping peaks were resolved by fitting a series of Lorentz functions to the corresponding experimental intensities in the Raman spectrum for each material. The mass fraction of the orthorhombic crystal component, X_c, was derived by the intensity of the CH_2 bending band at 1416 cm^{-1}. Similarly, the mass fraction of the amorphous region, X_a, was estimated from the CH_2 twisting vibrations. This amorphous region consists in two different fractions, a mobile amorphous part (liquid-like) and a transition region with molecules with a different conformation than in the pure liquid. The liquid-like mobile phase fraction, X_m, was obtained from the CH_2 rocking vibration, and then the fraction of the transition region was easily obtained as $X_{im} = X_a - X_m$. Finally, the fraction of material in the crystal interface was obtained as $X_{ic} = 1 - X_{im} - X_c - X_a$. We have considered that the material in the transition region and at the crystal interface form both part of the rigid amorphous phase, then $X_r = X_{im} + X_{ic}$. The results are listed in Table II. The difference found between w_{DSC} (obtained by DSC experiments) and X_c (by Raman experiments) is a common result in this type of systems. In Figure 5(a,b) is plotted the comparison of the values of the different phase mass fractions obtained from Raman measurements in the materials studied here (Table II) with other data from the literature obtained by PALS[27–29] and Raman measurements in polyolefins.[53,54] The agreement is good, as it can be observed in the figures. In general, an increase of the mobile amorphous fraction and a decrease in the interfacial fraction as crystal content decreases is observed. On the other hand, it is possible to calculate the corresponding mass phase fractions X_c, X_r, and X_m from the volume fractions obtained from the fit of the 3-phase model to the mechanical response (α, α_r, and α_m), taken from the crystal, interfacial (rigid), and amorphous phases density values from the literature: 1, 0.9, and 0.856 g/cm^3.[53,54] We have included these calculated fractions in Figure 5(c), together with our experimental values obtained by Raman experiments. The result in this figure indicates that there are differences in the fractional values found for both the mobile and the interfacial (rigid) amorphous phases, depending on the considered approach. Notwithstanding, it is worth to point out that the crystal content dependency of both amorphous phases fractional content obtained from the model is qualitatively similar to that obtained in the experiments. A continuous increase from nearly zero (at high α values) to one (in the amorphous limit) for the mobile amorphous phase is clearly observed. The rigid amorphous phase shows a different and characteristic behavior, reaching maximum values of around $X_r = 0.4$ at intermediate crystallinity and approaching to zero in both the amorphous and the crystalline limits. It is also worth to point out that the application of the mechanical model gives rise to lower values of the rigid amorphous fraction (or higher values of the amorphous mobile fraction) at a given crystal content than Raman infrared spectroscopy or PALS techniques.

The differences between the experimental and predicted elastic moduli are an indication of the inability of the proposed model to capture all the phenomena related to the rigid amorphous phase, although it improves some aspects not included in the previous ones. To illustrate this defect we have introduced to the model the measured values of the different phase fractions

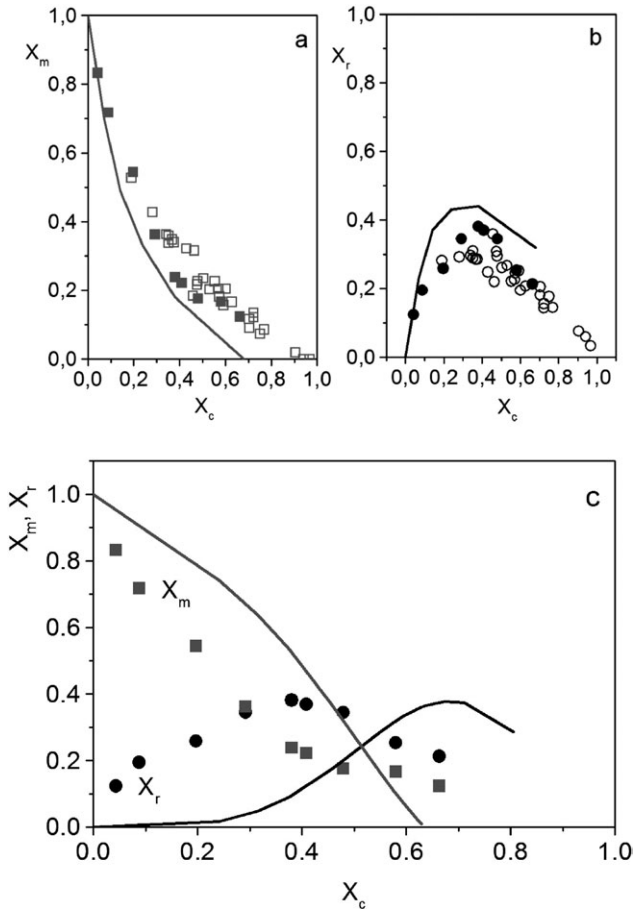

Figure 5. (a) Mobile (X_m) and (b) rigid (X_r) amorphous mass fractions versus mass crystalline fraction (X_c) obtained from Raman in the ethylene/1-hexene samples studied (solid symbols)[16] compared to those obtained from the literature by PALS (solid lines)[27–29] and Raman (open symbols).[53,54] In (c) the results obtained from Raman in our samples are compared to those obtained from the fitting to the mechanical model given by eq. (3).

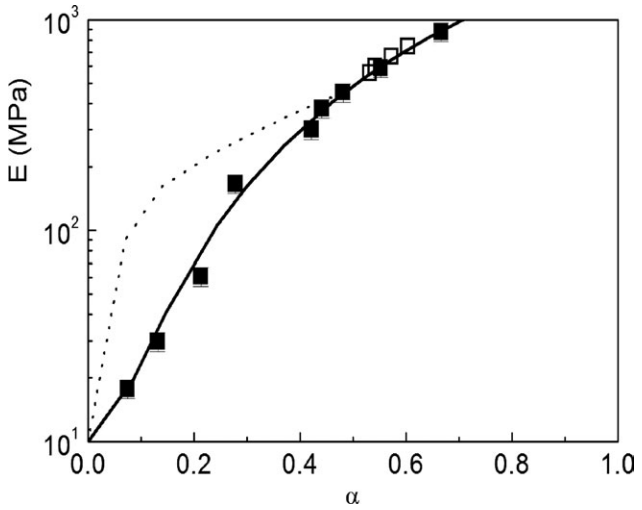

Figure 6. Application of the model given by eq. (3) using the fractional content of rigid amorphous, mobile amorphous, and crystal phases obtained by PALS[27–29] (dotted line) in similar polyolefins than the ethylene/1-hexene copolymers studied in this work (symbols and solid line).

obtained by PALS.[27–29] As it can be observed in Figure 6, the predicted elastic modulus is near one order of magnitude higher than the obtained experimentally in the samples with the lower crystal content. The difference observed may suggest a nonlinear coupling between both mobile and amorphous phases in this region or a softening of the rigid amorphous phase caused by the presence of an increasing amount of branches in the materials as crystallinity decreases.

CONCLUSIONS

The dependence of the elastic modulus on short chain branching content in the semicrystalline ethylene/1-hexene copolymers studied here is primarily modulated by the crystalline content. The comparison of the results obtained in pure homo, copolymers, and blends shows the same values of the modulus for the same crystalline content, although the blends display higher melting temperatures (and then crystal thickness) than the copolymers with the same branching content. The changes in the amorphous modulus, which can be extracted from measurements in the melt state, can neither explain the variation found in the measured elastic moduli. The strong dependence of this mechanical property with crystallinity is then ascribed to the presence of a rigid amorphous fraction, which gives rise to strong changes in the amorphous modulus with crystallinity and controls the mechanical properties. The experimental variation of the elastic modulus in these semicrystalline materials can be easily described by assuming a simple mechanical coupling among three phases; mobile amorphous, rigid amorphous, and crystalline. The model is only dependent on the volume fraction of the phases. The variation obtained for each amorphous fraction with crystalline content, by assuming a parallel–series coupling between amorphous and crystalline phases, is only qualitatively similar to that experimentally obtained by Raman infrared spectroscopy and PALS in ethylene/α-olefin copolymers.

ACKNOWLEDGMENTS

The authors thank the CICYT (MAT2009-12364) for the support of this investigation.

REFERENCES

1. Baer, H.; Hiltner, A.; Keith, H. D. *Science* **1987,** *235*, 1015.
2. Illers, K. H.; Kolloid Z. Z. *Polymer* **1973,** *251*, 394.
3. Martínez-Salazar, J.; Baltá Calleja, J. *Mater. Sci.* **1983,** *18*, 1077.
4. Popli, R.; Mandelkern, L. *J. Polym. Sci. Part. B:. Polym. Phys.* **1987,** *25*, 441.
5. Crist, B.; Fischer, C. J.; Howard, P. R. *Macromolecules* **1989,** *22*, 1709.
6. Peacock, A. J.; Mandelkern, L. *J. Polym. Sci. Part B: Polym. Phys. Ed.* **1990, 28, 1917.**
7. Krigas, T. M.; Carella, J. M.; Struglinski, M. J.; Crist, B.; Graessley, W. W.; Schilling, F. C. *J. Polym. Sci. Part B: Polym. Phys. Ed.* **1985,** *23*, 509.
8. Kennedy, M. A.; Peacock, A. J.; Mandelkern, L. *Macromolecules* **1994,** *27*, 5297.
9. Kennedy, M. A.; Peacock, A. J.; Failla, M. D.; Lucas, J. C.; Mandelkern, L. *Macromolecules* **1995,** *28*, 1407.
10. Simanke, A. G.; Galland, G. B.; Baumhardt Neto, R.; Quijada, R.; Mauler, R. S. *J. Appl. Polym. Sci.* **1999,** *74*, 1194.
11. Jordens, K.; Wilkes, G. L.; Rohlfing, D. C.; Welch, M. B. *Polymer* **2000,** *41*, 7175.
12. Ramos, J.; Peristeras, L. D.; Theodorou, D. N. *Macromolecules* **2007,** *40*, 9640.
13. Ramos, J.; Vega, J. F.; Theodorou, D. N.; Martínez-Salazar, J. *Macromolecules* **2008,** *41*, 2959.
14. Aguilar, M.; Vega, J. F.; Sanz, E.; Martínez-Salazar, J. *Polymer* **2001,** *43*, 9713.
15. Aguilar, M.; Vega, J. F.; Peña, B.; Martínez-Salazar, J. *Polymer* **2003,** *44*, 1401.
16. Otegui, J.; Vega, J. F.; Martin, S.; Cruz, V.; Flores, A.; Domingo, C.; Martínez-Salazar, J. *J. Mater. Sci.* **2007,** *42*, 1046.
17. Martín, S.; Vega, J. F.; Expósito, M. T.; Muñoz-Escalona, A.; Martínez-Salazar, J. *J. Appl. Polym. Sci.* **2008,** *109*, 1564.
18. Martín, S.; Vega, J. F.; Expósito, M. T.; Flores, A.; Martínez-Salazar, J. *Colloid. Polym. Sci.* **2011,** *289*, 257.
19. Chen, H. Y.; Chum, S. P.; Hiltner, A.; Baer, E. *J. Polym. Sci. Part B: Polym. Phys.* **2001,** *39*, 1578.
20. Boyer, R. F. *Macromolecules* **1973,** *6*, 288.
21. Cheng, S. Z. D.; Wunderlich, B. *Macromolecules* **1988,** *21*, 789.
22. Huo, P.; Cebe, P. *Colloid. Polym. Sci.* **1992,** *270*, 840.
23. Danch, A. *Fibres. Text. Eastern. Eur.* **2003,** *11*, 128.
24. Strobl, G. R.; Hagedorn, W. *J. Polym. Sci. Polym. Phys. Ed.* **1978,** *16*, 1181.
25. Glotin, M.; Mandelkern, L. *Colloid. Polym. Sci.* **1982,** *260*, 182.

26. Naylor, C. C.; Meier, R. J.; Kip, B. J.; Williamd, K. P. J.; Mason, S. M.; Conroy, N.; Gerrand, D. L. *Macromolecules* **1995,** *28*, 2969.
27. Kilburn, D.; Bamford, D.; Lüpke, T.; Dlubek, G.; Menke, T. J.; Alam, M. A. *Polymer* **2002,** *43*, 6973.
28. Dlubek, G.; Stejny, J.; Lüpke, T.; Bamford, D.; Petters, K.; Hübner, Ch.; Alam, M. A.; Hill, M. J. *J. Polym. Sci. Part B: Polym. Phys.* **2002,** *40*, 65.
29. Dlubek, G.; Bamford, D.; Rodríguez-González, A.; Bornemann, S.; Stejny, J.; Schade, B.; Alam, M. A.; Arnold, M. *J. Polym. Sci. Part B: Polym. Phys.* **2002,** *40*, 434.
30. Baltá Calleja, F. J.; Flores, A.; Di Marco, G.; Pieruccini, M. *Phys. Rev. B.* **2007,** *75*, 224201.
31. Baltá Calleja, F. J.; Flores, A.; Di Marco, G.; Pieruccini, M. *Phys. Rev. B.* **2009,** *79*, 019903.
32. Alvarez, C.; Šics, I.; Nogales, A.; Denchev, Z.; Funari, S. S.; Ezquerra. T. A. *Polymer* **2004,** *45*, 3953.
33. Pieruccini, M.; Ezquerra, T. A. *Eur. Phys. J. E.* **2009,** *29*, 163.
34. Pieruccini, M.; Flores, A. *Colloid. Polym. Sci.* **2010,** *288*, 365.
35. Quinn, F. A., Jr.; Mandelkern, L. *J. Am. Chem. Soc.* **1958,** *80*, 3178.
36. Wild, L.; Chang, S.; Shankernarayanan, M. J. *Polym. Prep.* **1990,** *31*, 270.
37. Gabriel, C.; Lilge, D. *Polymer* **2001,** *42*, 297.
38. Martín, S. Ph.D. Thesis, Universidad Complutense de Madrid, **2004.**
39. Boyd, H. *Polym. Eng. Sci.* **1979,** *14*, 1010.
40. Yamaguchi, M.; Miyata, H.; Tan, V.; Gogos, C. G. *Polymer* **2002,** *43*, 5249.
41. Vega, J. F. *Recent. Res. Dev. Macromol.* **2003,** *7*, 29.
42. Perez, J. *Polym. Sci. Ser. B.* **1998,** *40*, 17.
43. Halpin, J. C.; Kardos, J. L. *J. Appl. Phys.* **1972,** *43*, 2235.
44. Boyd, R. H. *J. Polym. Sci. Part B: Polym. Phys. Ed.* **1983,** *21*, 493.
45. Odajima, A.; Maeda, T. J. *Polym. Sci. C: Polym. Symp.* **1966,** *15*, 54.
46. Wobser, G.; Blasembrey, S.; Kollid Z. Z. *Polymer* **1970,** *241*, 985.
47. Sorenson, R. A.; Liau, W. B.; Kesner, L.; Boyd, R. H. *Macromolecules* **1988,** *21*, 200.
48. Struik, L. C. E. *Polymer* **1987,** *28*, 1521.
49. Struik, L. C. E. *Polymer* **1987,** *28*, 1534.
50. Takayanagi, M.; Uemura, S.; Minami, S. *J. Polym. Sci. C:. Polym. Symp.* **1964,** *5*, 113.
51. Takayanagi, M.; Imada; K.; Kajiyama, T. *J. Polym. Sci. C:. Polym. Symp.* **1966,** *15*, 263.
52. Mutter, R.; Stille, W.; Strobl, G. R. *J. Polym. Sci. Part B: Polym. Phys. Ed.* **1993,** *31*, 99.
53. Hedenqvist, M. S.; Angelstok, A.; Edsberg, L.; Larsson, P. T.; Geede, U. W. *Polymer* **1996,** *37*, 2887.
54. Neway, B.; Hedenqvist, M. S.; Mathot, V. B. F.; Gedde, U. W. *Polymer* **2001,** *42*, 5307.